University Library

MINERVA ACCESS

A gateway to Melbourne's research publications

Minerva Access is the Institutional Repository of The University of Melbourne

Author/s:
Cadusch, JJ;Meng, J;Craig, BJ;Shrestha, VR;Crozier, KB

Title:
Visible to long-wave infrared chip-scale spectrometers based on photodetectors with tailored responsivities and multispectral filters

Date:
2020-09-01

Citation:
Cadusch, J. J., Meng, J., Craig, B. J., Shrestha, V. R. & Crozier, K. B. (2020). Visible to long-wave infrared chip-scale spectrometers based on photodetectors with tailored responsivities and multispectral filters. Nanophotonics, 9 (10), pp.3197-3208. https://doi.org/10.1515/nanoph-2020-0114.

Persistent Link:
https://hdl.handle.net/11343/242409

License:
CC BY

Review

Jasper J. Cadusch, Jiajun Meng, Benjamin J. Craig, Vivek Raj Shrestha and Kenneth B. Crozier*

Visible to long-wave infrared chip-scale spectrometers based on photodetectors with tailored responsivities and multispectral filters

https://doi.org/10.1515/nanoph-2020-0114
Received February 14, 2020; accepted May 2, 2020; published online June 23, 2020

Abstract: Chip-scale microspectrometers, operational across the visible to long-wave infrared spectral region will enable many remote sensing spectroscopy applications in a variety of fields including consumer electronics, process control in manufacturing, as well as environmental and agricultural monitoring. The low weight and small device footprint of such spectrometers could allow for integration into handheld, unattended vehicles or wearable-electronics based systems. This review will focus on recent developments in nanophotonic microspectrometer designs, which fall into two design categories: (i) planar filter-arrays used in conjunction with visible or IR detector arrays and (ii) microspectrometers using filter-free detector designs with tailored responsivities, where spectral filtering and photocurrent generation occur within the same nanostructure.

Keywords: lab on chip; microspectrometers; nanophotonics; spectrometers.

1 Introduction

Recent history has seen the rapid miniaturization of optical components through the development of nanophotonic optical elements with functions akin to conventional optics such as lenses [1, 2], color filters [3, 4], polarizing beam splitters [5], wave-plates [6], spatial light modulators [7], photodetectors [8–10], and light sources [11, 12]. Now this trend has been extended to include more sophisticated, chip-scale optical systems such as interferometers [13, 14], systems to exploit quantum mechanical properties [15–17], as well as multispectral imaging systems [18, 19]. Here we review the recent progress in the development of chip-scale spectroscopy systems known as microspectrometers, developed to overcome the limitations of conventional systems such as diffraction grating-based spectrometers or Michelson interferometer-based Fourier transform infrared spectrometers (FTIR). These conventional benchtop systems typically weigh 1 to 50 kg and occupy footprints measured in tens of centimeters. They also often require precise alignment and damping from mechanical shocks and vibrations to reduce misalignment of optical or mechanical components and the incoming light beam. These requirements restrict these spectroscopic systems to laboratory settings and add to the total cost of the system. The need for collecting visible and infrared spectroscopic measurements in the field, both for scientific experiments and consumer applications provides motivation for the development of mechanically robust spectrometers with minimized extent and weight. A microspectrometer chip should typically not have moving any components, with the notable exception of microelectromechanical system (MEMS)-based examples [20–22], and as such are not as vulnerable to misalignment or mechanical failure due to shocks or vibrations. The dimensions and mass of the chips are on the order of millimeters and grams respectively. The compact size and inherent robustness of chip-scale spectrometers potentially allows for the deployment of microspectrometers in handheld consumer devices, integrated into mobile telephones [23–25], or augmented reality visualizers [26], incorporated into remote sensing systems on air-, sea- or space-borne unmanned vehicles [27–30], or used for systems- or quality-control in industrial settings [31].

Broadly, recently demonstrated chip-scale microspectrometers can be placed into one of two distinct design categories: (i) the filter-array-detector-array (FADA) microspectrometer and (ii) the filter-free microspectrometer. The

***Corresponding author: Kenneth B. Crozier**, Department of Electrical and Electronic Engineering, The University of Melbourne, Melbourne, Victoria, 3010, Australia; School of Physics, The University of Melbourne, Melbourne, Victoria, 3010, Australia; and Australian Research Council Centre of Excellence for Transformative Meta-Optical Systems Melbourne, Victoria, 3010, Australia, E-mail: kenneth.crozier@unimelb.edu.au
Jasper J. Cadusch and Jiajun Meng: Department of Electrical and Electronic Engineering, The University of Melbourne, Melbourne, Victoria, 3010, Australia
Benjamin J. Craig and Vivek Raj Shrestha: School of Physics, The University of Melbourne, Melbourne, Victoria, 3010, Australia

Open Access. © 2020 Jasper J. Cadusch et al., published by De Gruyter. This work is licensed under the Creative Commons Attribution 4.0 International License.

FADA approach utilizes a planar optical element which consists of a set of spectral filters each with a unique transmission spectrum. Some of the nanophotonic spectral filters used in FADA microspectrometers include thin film (etalon) bandpass or linear variable filters with transmission bands in the visible [32–36], and infrared [37], plasmonic nanoantennas [38, 39], plasmonic nanoapertures resonant in the mid- and long-wave infrared (M/LWIR) spectral bands [40, 41], photonic crystal (PhC) slabs [20, 42], on-chip waveguide coupled disordered scattering media [43, 44] and colloidal quantum dot (QD) optical absorption based filters [45]. The transmission spectrum of each nanophotonic filter in the filter array is measured via a grating-based or an FTIR-based spectrometer in the lab and stored for later use. The filter arrays are then attached to an array of photosensitive detectors such as photodiodes [44], charge-coupled device (CCD) or complementary metal-oxide semiconductor (CMOS) camera sensors [39, 42, 45], or linear array of pyroelectric sensors for MWIR or LWIR applications [37]. The current or voltage signals generated in each pixel in the detector array as a response to illumination thus depends upon the (unknown) spectral content of the incoming light, the measured transmission functions of the filter in front of the detector pixels and the intrinsic responsivity of the detector pixels themselves.

An alternative to the FADA approach to microspectrometer design has emerged recently, that is, the filter-free microspectrometer design. In designs of this type the wavelength discrimination and photonic-to-electronic signal conversion takes place within the same nanostructure. Microspectrometer chips have been formed from a single compositionally-engineered semiconductor nanowire where the elemental composition and thus band gap energy and optical absorption spectrum vary with position along the nanowire [46]. Other examples consist of sets of structurally colored silicon PIN photodiodes comprised of either arrayed vertical nanowires [47] or high contrast gratings (HCGs) [48], where each pixel in the spectrometer has a unique responsivity, tailored through control of the geometry. These three filter-free designs represent in some sense the ultimate miniaturization of spectrometers, as they consist of only one component. For filter-free designs the responsivity of each pixel is measured carefully and stored. To measure the spectrum of an incident beam the photocurrents light generates in each pixel are measured and the pre-measured responsivity library can then be used, along with an appropriate algorithm to reconstruct the unknown spectrum of light illuminating the chip.

Figure 1(a–c) shows a typical configuration schematic and transmitted signal for a conventional grating-based spectrometer, (a), a FTIR spectrometer (b) and a FADA microspectrometer (c). The grating spectrometer measures a spectrum by scanning the angle of the grating to sweep the diffracted light across a slit in front of a photodetector or alternatively by projecting the diffraction pattern directly onto a CCD matrix or focal plane array. The further the distance of the grating from the detector or slit, where the higher the spectral resolution. The spectrum is recovered simply by reading out the photoresponse at each grating angle or the intensity from each pixel in the CCD image. This is possible due to the narrowband (delta function-like) transmission of the grating and slit combination. FTIR spectrometers use a suitable infrared photodetector and a scanning mirror in a Michelson interferometer to measure an interferogram of the incoming light. A Fourier transform then allows the user to find the light spectrum.

FADA and filter-free microspectrometers can often have transmission or responsivity spectra that are broadband and of a highly dispersive, but deterministic, form. In this case a direct photoresponse read-out of each pixel or a simple Fourier transform cannot recover the incident spectrum. Instead a suitable reconstruction algorithm must be chosen to find the spectrum. The measured photoresponse, $I_n(\lambda)$, of the n^{th} detector pixel will be given by

$$I_n(\lambda) = \int_{\lambda_1}^{\lambda_2} R_n(\lambda) S(\lambda) d(\lambda) \tag{1}$$

where $R_n(\lambda)$ is the responsivity of the n^{th} pixel and $S(\lambda)$ is the incident spectral density [39]. For FADA microspectrometers $R_n(\lambda) = T_n(\lambda) R_0(\lambda)$, where $T_n(\lambda)$ is the transmission of the n^{th} filter and $R_0(\lambda)$ is the intrinsic responsivity of the detector array. To estimate the incident spectrum, $S(\lambda)$ using equation (1) and real experimental data there exist several linear regression methods. Researchers have used techniques such simulated annealing [44, 48, 49], recursive least squares [38, 40, 47], Tikhonov (L_2) regularization [39, 45, 48, 50], Lasso (L_1) regularization [51], as well as non-negative least squares [47, 52], since $S(\lambda)$ is always non-negative. These methods are used in place of direct matrix inversion [49] or computing the Moore–Penrose inverse or using singular-value decomposition method as the regularization parameter introduced helps reduce the impact of random noise and measurement errors in either of the measured photoresponses or the responsivities [49]. The spectral resolution of a particular microspectrometer is difficult to estimate because of the differences in these reconstruction techniques. In general, however, it has been shown that the performance of a microspectrometer relying on a reconstruction algorithm improves with increasing number of filters [46] and performs best when the transmission spectra of the filter set

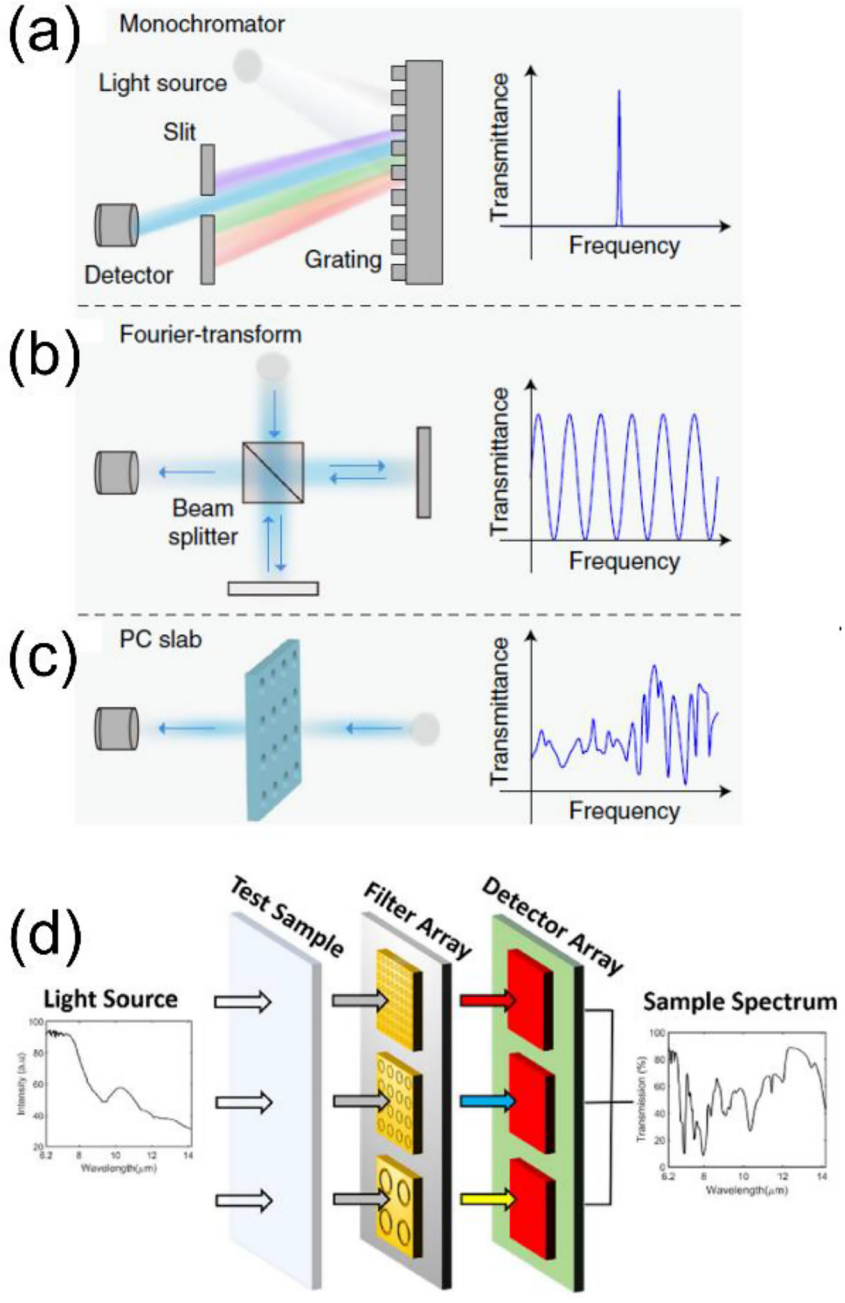


Figure 1: Schematics and typical spectral responsivity of (a) grating spectrometer data point, (b) Fourier transform infrared spectrometers (FTIR) spectrometer and (c) photonic crystal (PhC) slab filter-array-detector-array (FADA) microspectrometer pixel. (d) FADA microspectrometer experimental configuration. Reprint permission obtained from [40, 42].

and therefore the responsivities of each pixel have as little cross-correlation as possible [53].

2 Filter-array-detector-array based microspectrometers

2.1 Background

Nanophotonic FADA microspectrometers are attractive for researchers as they are able to leverage current imaging technologies such as CMOS or CCD camera sensors and adapt them into microspectrometers by adding their own custom filter arrays. These commercial sensor arrays provide benefits such as a large number of pixels, on-board electronics to digitize and read-out intensity values, high dynamic range and sensitivities. Early versions of microspectrometers were commercial imaging sensors equipped with linear variable filters (LVF) [34–36], or a set of Fabry–Perot etalon bandpass filters [32]. These filter arrays were straightforward to fabricate, requiring only thin film deposition and no lithographic fabrication steps in the case

of LVFs or photolithography to define the etalon pixels. These types of optical filters produce narrowband transmission spectra and as such do not usually require the implementation of a reconstruction algorithm, as a direct pixel read-out method is applicable.

The development of spectral reconstruction algorithms for broadband filter arrays [39, 52] allowed for filter arrays with more sophisticated transmission spectra to be used in FADA microspectrometer configurations. These include using chemically synthesized colloidal QDs as absorptive filters [45], PhC slabs [20, 42] and plasmonic nanoantennas [38] or apertures [40]. The FADA approach to measuring test sample transmission spectra is outlined in [40] and reproduced in Figure 1(d). Light from a source, with its own characteristic spectrum is passed through a test sample, where the source spectrum is modified by the wavelength dependent absorption and scattering of the sample. Light from the sample is then filtered by the nanophotonic filter array and collected by a set of suitable detectors. The measured photoresponse is then used with the known transmission spectra of each filter and that of the source to find the sample's transmission spectrum.

2.2 Quantum dot absorptive filter array

Figure 2(a) shows a color photograph of a set of chemically synthesized core–shell colloidal Cadmium sulfide (CdS)/Cadmium selenide (CdSe) QDs of varying composition and radii [45]. Each circular aggregate of QDs forms an absorptive spectral filter, where all the QDs in the filter have the same radius and composition. By varying the growth conditions, it was possible for the authors to create 195 different QD filters with distinct, broadband transmission spectra, a selection of which can be seen in Figure 2(b). The QDs are then encapsulated in a polyvinyl butyral film and each of the 195 filters transmission characterized. The QD filter film is then attached to a commercial monochrome silicon CCD camera shown in Figure 2(c).

Broadband test spectra were generated, and images were captured with the QD-FADA camera. Each pixel in the captured image was then either registered to a particular QD filter or not used as the light passes through the membrane unfiltered. By using least-squares L_2 regularization the authors were able to reconstruct visible spectra ranging from 400 to 600 nm in wavelength as shown in Figure 2(d–g). This QD microspectrometer is also capable of reconstructing narrowband spectra, down to linewidths of 3 nm. The stability of the QD filter array was characterized by performing measurements of the same narrowband test spectra 6 months apart. The authors found no degradation in the function of the QD microspectrometer after this time period.

One of the limitations of using QDs as absorptive filters in a FADA microspectrometer include the heavy metals used to make these QDs are toxic and may in future be

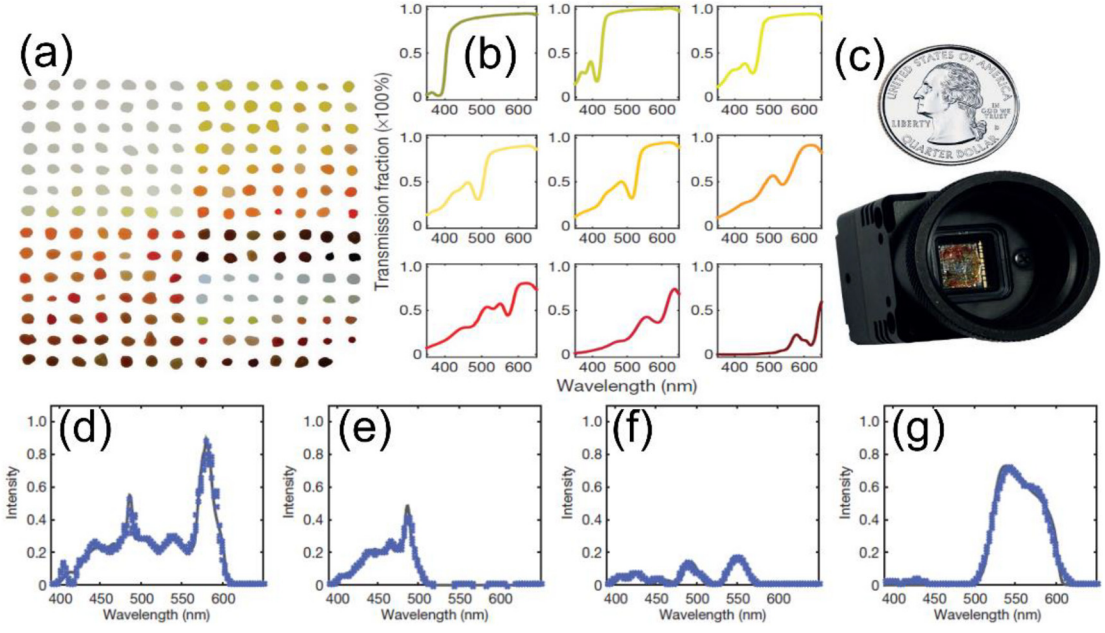


Figure 2: Colloidal quantum dot (QD) FADA microspectrometer. (a) 195 absorption filters formed from uniquely sized QDs embedded in a polyvinyl butyral film. Transmission spectra of nine of the QD filters in the array (b). Filter array integrated into a commercial charge-coupled device (CCD) camera (c). Measured (crosses) and reference (solid line) spectra using the QD microspectrometer (d)-(g). Reprint permission obtained from [45].

phased out of use because of this. Furthermore, the material choice limits the spectral range to around the band gap energies of the QDs, so that the microspectrometer range is limited by the filter array design, not by the intrinsic responsivity of the detector array. Finally, the authors evaluate the viability of a QD-FADA microspectrometer with 147 filters instead of 195 filters and found the test spectral reconstructions to be less accurate. This suggests limited viability for mass production as in this design each spectrometer will need 195 different QD synthesis steps. Nevertheless, filters based on QD absorption have natural advantages over the "top-down" fabricated filters as their transmission spectra have no angular or polarization dependence, whereas thin film, PhC slab, plasmonic nanoantenna and grating-based spectrometers often do.

2.3 Plasmonic and photonic crystal slab filter arrays

PhC slab filters consist of regular arrays of air holes in a dielectric film, where the transmission through the slab is determined by the array period, lattice constant and diameter of the holes. Figure 3(a) shows a schematic of a PhC-FADA microspectrometer, where the filter array consists of 36 distinct PhC designs etched into 500 nm of silicon-on

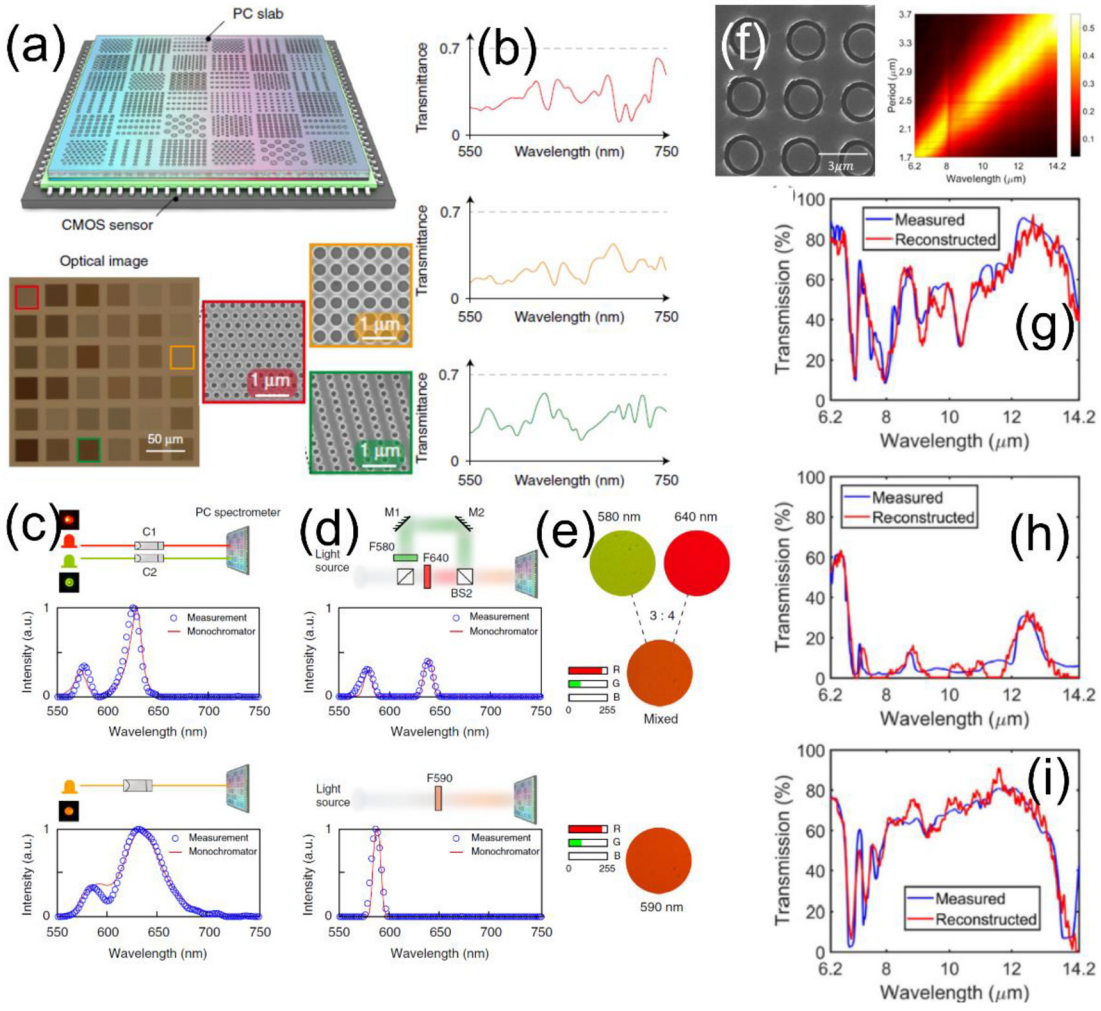


Figure 3: PhC filters integrated onto a CMOS sensor array (a). Transmission spectra of three of the PhC filters (b). Reconstructed (blue) and reference (red) LED spectra (c). PhC slab microspectrometer can be used to distinguish two metameric colored light sources (reconstructed and reference spectra (d) and appearance and Red-green-blue (RGB) color values (e)). scanning electron microscope (SEM) and measured transmission spectra of LWIR filter array microspectrometer based on plasmonic apertures in a gold film. Reconstructed (red) and reference transmission spectra (blue) of various plastics: cellophane (g), polyvinyl chloride (PVC) (h) and Polyethylene (PE) (i). Reprint permission obtained from [40, 42].

sapphire and attached to a commercial CMOS sensor [42]. Simulations carried out suggested that increasing the number of filters beyond 30 had little effect on reducing the mean-squared-error of the simulated spectrometer chip's spectral reconstructions. Each filter pixel is 32×32 μm and the total filter array is just 200×200 μm. Figure 3(b) shows the transmission spectra for three of the PhC filter arrays. The complex nature of the transmission spectra is exploited here to reduce the cross-correlation of each filter's transmission, which has been shown to improve microspectrometer accuracy [53]. The PhC filter array has less than 70% transmission, perhaps due to absorption in the silicon used as the filter material, this reduces the overall sensitivity of the spectrometer chip, compared to a grating spectrometer. Here L_2 regularization is used to estimate the incident light spectrum. Figure 3(c) shows the PhC-FADA spectrometer chip measured spectra as well as reference spectra of light from two different LED light sources. The results are in good agreement. The spectrometer chip was also used to measure monochromatic light with wavelengths from 550 to 750 nm. The spectral resolution for such measurements is claimed to be about 1 nm across this wavelength range. An interesting application of this spectrometer is shown in Figure 3(d), (e). Here the authors generate two beams with distinct spectra (see 3(d)) but appear to have the same color and indeed have the same Red-green-blue (RGB) color values. The PhC-FADA spectrometer is able to easily distinguish between these metameric beams, something a color CMOS camera could not do. The PhC slab filter array does, however, have a clear drawback: the transmission spectra are highly sensitive to the angle of incidence of the incoming light. The authors evaluate this and find that the reconstructed spectrum is accurate only up to a difference of 3° angle of incidence between the transmission spectra measurements of each filter (calibration) and the beam under test.

Unlike PhC slab filters, many plasmonic filter arrays designs with transmission spectra insensitive to polarization angle and robust to angle of incidence have been developed. Figure 3(f) shows a scanning electron microscope (SEM) image of such a design. The filter design here consists of an array of coaxial nanoapertures in a 140 nm gold film on an undoped silicon substrate. The measured transmission spectra of a set of coaxial nanoapertures designed to filter LWIR light is also shown in Figure 3(f). The transmission peaks are tuned from 6 to 14 μm by varying the array period and aperture dimensions, with a peak transmission around 50%. The full-width-half-maximum of the transmission peaks are broad, around 1–2 μm and greater. Nevertheless researchers were able to use a set of 101 of these plasmonic filters to create a LWIR FADA microspectrometer [40]. The transmission of each filter array characterized using an FTIR microscope and spectrometer. In this case a detector array is synthesized by using the detector in the FTIR spectrometer and integrating the signal to give a scalar "photocurrent" reading for each filter and for each sample spectrum. A recursive least squares method is used to recover first the spectrum of the blackbody source within the FTIR system and then subsequently used to reconstruct the transmission spectra through several plastic films, shown in Figure 3(g–i). The measured and reference spectra are in good agreement, even for the fine absorption lines of the bonds in the polymer films, which is important for material identification in remote sensing applications. The angular sensitivity of the filter array is investigated through simulation. The transmission is shown to have a small reduction in magnitude up to 10° angle of incidence, but the transmission peak wavelengths are stable. This work and other demonstrations of MWIR and LWIR microspectrometers [38, 41], hold great promise for remote sensing due to the 10^4-fold reduction in mass and dimensions of these designs compared to conventional FTIR spectrometer systems and the importance of this spectral region in materials identification including noxious gases, polymers and explosives.

3 Filter-free chip-scale microspectrometers

3.1 Background

Recently a new class of microspectrometer has emerged, where instead of replacing a dispersive element such as a Michelson interferometer or diffraction grating with a planar nanophotonic filter, the dispersion (and hence wavelength discrimination) occurs within the photodetectors themselves. Two methods of tailoring detector responsivities without the use of external filters have been put forward: (i) structural coloration of PIN photodiodes and (ii) material composition engineering to spatial tailor detector band gap energy. These approaches to microspectrometers again rely upon reconstruction algorithms to estimate incident spectra from measured photocurrents and known (calibrated) responsivities.

3.2 Structurally colored nanophotonic photodiode arrays

Silicon can be structurally colored by reactive ion etching nanophotonic elements such as arrays of vertical

nanowires or sub-diffractive high contrast gratings. In both instances particular wavelengths of light will be strongly absorbed in the silicon, while other wavelengths are reflected or transmitted through the structure. Which wavelengths will be absorbed is determined by the leaky waveguide modes supported by the nanophotonic nanostructures, which in turn is determined by the array period and waveguide or nanowire cross-section. A range of these geometric parameters can be set within the one lithographic step. By creating a set of these arrays with various structural color in a PIN doped silicon substrate it is possible to create a filter-free microspectrometer chip.

Figure 4(a) shows a nanowire array based microspectrometer developed by researchers at the University of Melbourne [48]. Each colored square is a uniform array of nanowires of a specific radius, ranging from 60 to 175 nm, here the period is fixed and the radius of the nanowires controls the absorption of light at each pixel. The structural color provided by the silicon nanowires has been exploited to create a color printed image of the University's emblem. Figure 4(b) shows an SEM image of one of the nanowire pixels after reactive ion etching and before planarization and metallization has been carried out. Each nanowire in an array is a vertical PIN photodiode, with 200 nm p + layer on top of 2 μm of lightly doped silicon region and then 500 nm of n + doped silicon. To make electrical contact with the top (p + layer) of each nanowire an epoxy planarization layer is used, then etched back to reveal just the nanowire tips and a thin transparent conductive oxide (TCO) deposited. Metal contacts, leads and pads are also

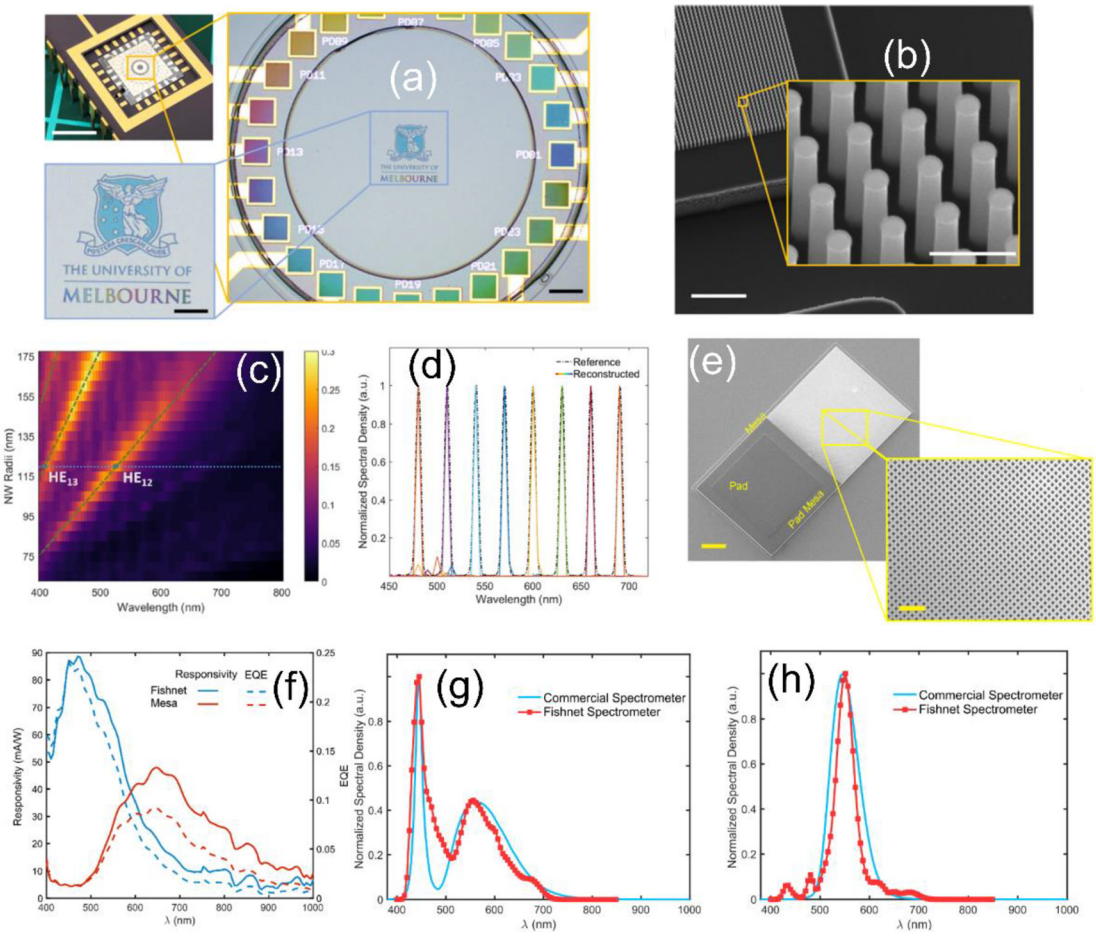


Figure 4: Optical (a) and SEM (b) images of a silicon nanowire array microspectrometer (scale bars are: (clockwise from top left) 5 mm, 200 and 100 μm in (a) and 10 and 1 μm (inset) in (b)). Each pixel consists of an array of nanowires of a particular radius, varying the radius changes the structural coloration. Measured nanowire detector responsivities (c) and reconstructed and reference (dashed line) sample spectra (d). SEM images of a silicon fishnet pixel (e) (scale bars: 50 and 2 μm inset). Pixel responsivity and external quantum efficiency (EQE) spectra from both the fishnet and mesa detectors (f). Fishnet microspectrometer measured (red) and reference (blue) broad- and narrow-band sample spectra (g) and (h). Reprint permission obtained from [47, 48].

deposited. Each nanowire array also sits on a mesa, which is itself a planar PIN photodiode connected in series with the nanowire diodes. Current measured with a positive bias is mostly photocurrent from the nanowire array, and when this bias is reversed, photocurrent from the mesa is measured. This allows for two distinct detectors within the one on-chip footprint. The responsivities of the nanowire and mesa detectors are complementary since any light that is not absorbed by the nanowire array is absorbed by the mesa detector below. Figure 4(c) shows the external quantum efficiency (EQE) of each of the 24 nanowire pixels in the microspectrometer chip. Peak EQE values of 30% occur at spectral positions corresponding to leaky hybrid (HE) waveguide modes. Corresponding reduction in EQE occurs in the mesa diodes. After calibration, the spectrometer chip was used to measure narrowband light sources across the visible spectrum as shown in Figure 4(d). The spectral reconstructions in this case employed L_1 regularization, which is well suited to sparse spectra [51]. From these measurements the authors estimate the spectrometers resolution to be around 5 nm. Broad spectra were also measured using this design, but instead employed the RLS method, as it was found to outperform L_1 regularization for these broader sources.

Figure 4(e) shows an SEM image of a fishnet pixel, another type of structurally colored silicon detector [48]. In this case each diode is comprised of a vertically oriented set of two interleaved orthogonal waveguide arrays. Unlike its nanowire counterpart, the interleaved design of the fishnet pixels means there is no need for planarization, etch-back, and TCO deposition. A combination of waveguide theory calculations and finite element method simulations suggest this structure can have near-unity absorption for wavelengths of light near each HCG mode cut-off wavelength, which are determined by the array period and width of each waveguide. The fishnet pixels are also etched into a PIN doped silicon substrate and sits upon its own mesa photodetector. Figure 4(f) shows the responsivity and EQE spectra of one of the 20 pixels in the fishnet microspectrometer chip for both fishnet and mesa detector. The fishnet detectors have peak sensitivities ranging from 400 to 620 nm. Here the mesa detectors are used to extend the operating range of the microspectrometer chip up to 800 nm, covering the entirety of the visible spectrum. After measuring the responsivities of each pixel and then the photocurrents generated by test spectra in each pixel a supervised machine learning algorithm is used to estimate the incident spectrum. The first stage consists of L_2 regularization, the result of which is then fed into a simulated annealing stage to improve the estimated spectrum. Spectral measurements of a white LED and the same LED filtered with a bandpass filter are shown in Figure 4(g), (h), the results are in agreement with the reference spectra.

3.3 Single nanowire spectrometers via material composition engineering

The filter-free microspectrometer designs discussed thus far have all been based upon sets of individual photosensitive pixels, each with their own distinct responsivity spectra, which also can have varied response to illumination conditions such as the angle of incidence. Recently, however, it has been demonstrated that a filter-free microspectrometer can be formed from a single semiconductor nanowire, without the need for structural coloring [46]. In this design the nanowire is grown via a chemical vapor deposition process and is composed of compositionally graded CdS_xSe_{1-x}. One end of the 100 μm long nanowire is mostly CdS, the other end is mostly CdSe with a smooth transition of material composition in between. This means the band gap energy spatially varies from 1.74 eV (CdSe) to 2.42 eV (CdS) along the nanowire's length and hence the absorption spectrum of the semiconductor nanowire also varies spatially. Figure 5(a) shows a photoluminescence (PL) color image and emission spectra from different points along the nanowire, where the change in emission color and wavelength indicate a change in band gap energy. After growth the nanowires are placed on a silica substrate and an array of electrical contacts are deposited to form a linear array of detectors with unique responsivities. This is shown in Figure 5(b), where each region of nanowire between to metal electrodes forms one of the 38 microspectrometer detector units. Unlike the previously discussed examples of photodiode-based filter-free microspectrometers, here each unit acts as a photoconductor, but judicious choice of the metal contacts could allow for Schottky photodiodes to be formed. A thin Al_2O_3 passivation layer is then deposited to encapsulate and protect the nanowire. Figure 5(c) shows the normalized responsivity spectra from each detector unit measured with a 0.5 V bias. The spectrometer operational range is just over 100 nm wide, ranging from 510 to 620 nm, this is restricted by the band gap energies of the bulk semiconductors chosen to grow the nanowire from. This limitation is not easy to overcome as the growth of compositionally graded nanowires is not possible with just any combination of semiconductors, however, the authors do suggest several alternative combinations. Spectra measured with the nanowire spectrometer is shown in Figure 5(d), where the results agree well with the reference spectra. Here L_2 regularization is used to reconstruct

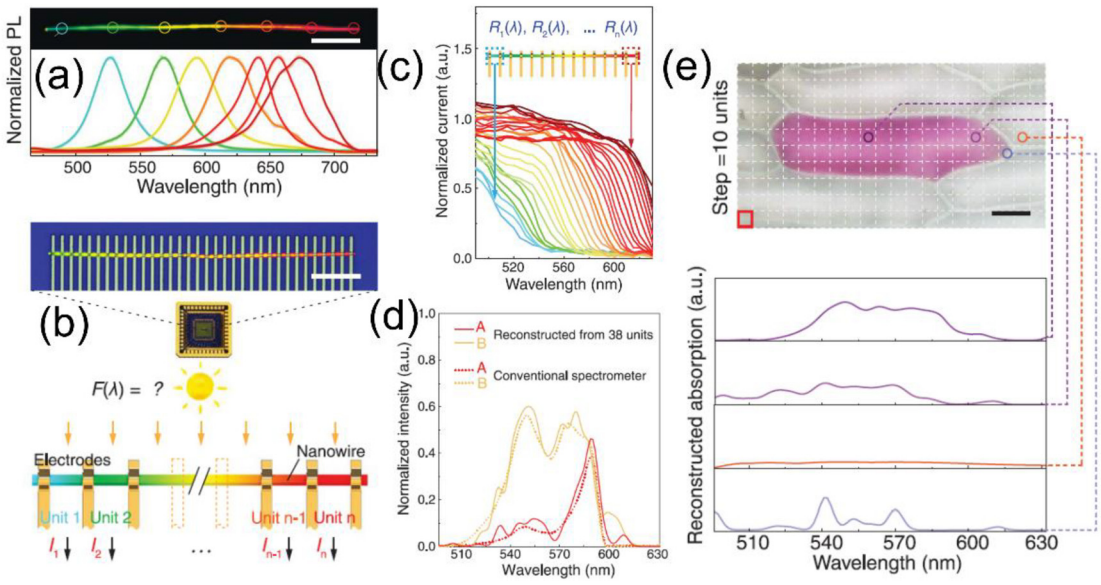


Figure 5: Photoluminescence image and position-dependent spectra (a) from a single CdS_xSe_{1-x} nanowire (scalebar 20 μm). Optical image and schematic of the single nanowire microspectrometer (b) (scalebar 10 μm). Measured position-dependent responsivity spectra (c) and (d) measured (solid) and reference (dashed) sample spectra. Reconstructed absorption scanning spectra (e) from different locations within an onion cell, measured with a single nanowire microspectrometer. Reprint permission obtained from [46].

incident spectra but the algorithm also has a method for detecting erroneous photocurrent measurements, by comparing the mean photocurrent to its standard of deviation. If a detector fault occurs or a particular photocurrent value is far outside what is expected the algorithm will exclude that detector from the reconstruction. Even though the total detector number is then reduced, by excluding data from suspicious detectors the reconstruction algorithm has improved accuracy and robustness to measurement error. The stated spectral resolution of this microspectrometer is 1 nm.

This nanowire microspectrometer chip can also operate as a scanning hyperspectral imaging sensor and provide in situ spectral imaging. Since each detector in the spectrometer is only 2.5 μm wide, scanning microscopy techniques can be used without the need of a pinhole aperture or single-mode optic fiber. Figure 5(e) shows a micrograph of a few red onion cells and the locations of absorption measurements. Below that are four distinct absorption spectra measured with the single nanowire microspectrometer chip. This application could be very useful for cytobiology and biomedicine research, where detailed spectral data registered to a location within a microscope image of each cell will provide important information about bio-composition and chemical concentrations and could be used to augment machine vision in artificial neural network powered experiments [54, 55].

4 Conclusions and outlook

Lightweight, low-profile microspectrometer chips operational across the visible to LWIR spectrum will allow for novel spectroscopy applications for industrial use, consumer electronics and scientific purposes. The potential for robust low-cost, low power consumption field-deployable spectrometers will enable spectroscopy in settings currently inaccessible to or inappropriate for conventional bulky grating or FTIR spectrometers. This extreme miniaturization of spectrometers to chip-scale has been enabled by developments in signal processing and machine learning algorithms as well as the emergence of nanophotonic devices for the compact and tunable filtering of light. By carefully measuring the optical properties, such as the transmission, absorption or responsivity of each element or pixel in the microspectrometer chip, it is possible to use one of several reconstruction algorithms to determine an unknown spectrum incident upon the chip from the of intensity or photocurrent values the light generates at each pixel.

One of the more flexible approaches to designing microspectrometers chips is the FADA microspectrometer, where an array of nanophotonic spectral filters sits above a detector matrix such as a CCD sensor or pyroelectric sensor array. Here the intended application will determine both the form of the filter array and the choice of detector array.

For example, to discriminate between plastics such as Polyethylene (PE) and polyvinyl chloride (PVC) in a machine vision application, one can compare their absorption spectra in the LWIR region of the spectrum. A microspectrometer designed for this purpose could use a set of coaxial plasmonic apertures in a gold film above an array of $Hg_{1-x}Cd_xTe$ (MCT) photodiodes or vanadium oxide (VOx) microbolometers. Alternatively, the same FADA approach can be used create a visible spectrometer for colorimetry by adding a set of absorptive QD filters, or a PhC slab to a silicon CMOS sensor. In this case each choice of filter array has its drawbacks that need to be considered, for example QDs can be toxic to both humans and the environment whereas the PhC filters can be very sensitive to the angle of incidence of incoming light.

A recent novel approach to the development of microspectrometers is the filter-free design, where the responsivity of each on-chip detector is tailored and unique. This approach in some sense represents the ultimate miniaturization of spectrometers, where the spectral filtering and detection occur at the same point in space, within the same element of the device. This has been achieved by exploiting the structural color property of high refractive index semiconductors such as silicon, where arrays of nanophotonic structures such as nanowires or fishnet arrays are patterned into PIN doped junctions. A filter-free spectrometer can also be realized by spatially tailoring the material composition and therefore band gap energy of a single nanowire and forming an array electrical contact along its length. These designs can allow for extra, novel functionalities such as image printing with structurally colored silicon or scanning spectral imaging with a single nanowire microspectrometer.

The benefits of chip-scale spectrometers for both visible and infrared applications are only just beginning to be realized with several novel designs published in the last few years. All of which have been enabled by advances in nanophotonics and spectral reconstruction techniques. The next frontier in size reduction is to develop microspectrometers based upon the integration of nanophotonic structures with visible and infrared photodetectors based on 2D materials.

Acknowledgments: This work was supported by the Australian Research Council (LP160100959, DP150103736, DP180104141, and FT140100577), by the Defense Advanced Research Projects Agency (DARPA) (HR0011-16-1-0004), by Palette and by VESKI.

Author contribution: All the authors have accepted responsibility for the entire content of this submitted manuscript and approved submission.

Research funding: See Acknowledgments.

Employment or leadership: None declared.

Honorarium: None declared.

Conflict of interest statement: The authors declare no conflicts of interest regarding this article.

References

[1] J. S. Park, S. Zhang, A. She, et al., "All-glass, large metalens at visible wavelength using deep-ultraviolet projection lithography," *Nano Lett.*, vol. 19, no. 12, pp. 8673–8682, 2019.

[2] E. Schonbrun, K. Seo, and K. B. Crozier, "Reconfigurable imaging systems using elliptical nanowires," *Nano Lett.*, vol. 11, no. 10, pp. 4299–4303, 2011.

[3] T. Ellenbogen, K. Seo, and K. B. Crozier, "Chromatic plasmonic polarizers for active visible color filtering and polarimetry," *Nano Lett.*, vol. 12, no. 2, pp. 1026–1031, 2012.

[4] T. D. James, P. Mulvaney, and A. Roberts, "The plasmonic pixel: Large area, wide gamut color reproduction using aluminum nanostructures," *Nano Lett.*, vol. 16, no. 6, pp. 3817–3823, 2016.

[5] M. Khorasaninejad, and K. B. Crozier, "Silicon nanofin grating as a miniature chirality-distinguishing beam-splitter," *Nat. Commun.*, vol. 5, no. 1, pp. 1–6, 2014.

[6] J. J. Cadusch, T. D. James, and A. Roberts, "Experimental demonstration of a wave plate utilizing localized plasmonic resonances in nanoapertures," *Optics Express*, vol. 21, no. 23, pp. 28450–28455, 2013.

[7] S. Q. Li, X. Xu, R. M. Veetil, V. Valuckas, R. Paniagua-Domínguez, and A. I. Kuznetsov, "Phase-only transmissive spatial light modulator based on tunable dielectric metasurface," *Science*, vol. 364, no. 6445, pp. 1087–1090, 2019.

[8] H. Park, and K. B. Crozier, "Multispectral imaging with vertical silicon nanowires," *Sci. Rep.*, vol. 3, pp. 2460, 2013.

[9] H. Park, Y. Dan, K. Seo, et al., "Filter-free image sensor pixels comprising silicon nanowires with selective color absorption," *Nano Lett.*, vol. 14, no. 4, pp. 1804–1809, 2014.

[10] E. Panchenko, J. J. Cadusch, T. D. James, and A. Roberts, "Plasmonic metasurface-enabled differential photodetectors for broadband optical polarization characterization," *ACS Photonics*, vol. 3, no. 10, pp. 1833–1839, 2016.

[11] M. Molaei, M. Marandi, E. Saievar-Iranizad, et al., "Near-white emitting QD-LED based on hydrophilic CdS nanocrystals," *J. Lumin.*, vol. 132, no. 2, pp. 467–473, 2012.

[12] C. Chase, Y. Rao, W. Hofmann, and C. J. Chang-Hasnain, "1550 nm high contrast grating VCSEL," *Optics Express*, vol. 18, no. 15, pp. 15461–15466, 2010.

[13] L. Bi, J. Hu, P. Jiang, et al., "On-chip optical isolation in monolithically integrated non-reciprocal optical resonators," *Nat. Photonics*, vol. 5, no. 12, p. 758, 2011.

[14] A. L. Washburn and R. C. Bailey, "Photonics-on-a-chip: Recent advances in integrated waveguides as enabling detection elements for real-world, lab-on-a-chip biosensing applications," *Analyst*, vol. 136, no. 2, pp. 227–236, 2011.

[15] K. Wang, J. G. Titchener, S. S. Kruk, et al., "Quantum metasurface for multiphoton interference and state reconstruction," *Science*, vol. 361, no. 6407, pp. 1104–1108, 2018.

[16] G. Li, S. Zhang, and T. Zentgraf, "Nonlinear photonic metasurfaces," *Nat. Rev. Mater.*, vol. 2, no. 5, pp. 1–14, 2017.
[17] S. Xiao, J. Wang, F. Liu, S. Zhang, X. Yin, and J. Li, "Spin-dependent optics with metasurfaces," *Nanophotonics*, vol. 6, no. 1, pp. 215–234, 2016.
[18] D. J. Garrood, N. N. Shah, D. L. Barker, and H. A. Schmitt, Multispectral Imaging Chip Using Photonic Crystals, USA, US20060054780A1, 2006.
[19] T. Maier and H. Brueckl, "Multispectral microbolometers for the midinfrared," Optics letters, 35 (2010) 3766-3768.
[20] Ž. Zobenica, R. W. van der Heijden, M. Petruzzella, et al., "Integrated nano-opto-electro-mechanical sensor for spectrometry and nanometrology," *Nat. Commun.*, vol. 8, no. 1, pp. 1–8, 2017.
[21] L. P. Schuler, J. S. Milne, J. M. Dell, and L. Faraone, "MEMS-based microspectrometer technologies for NIR and MIR wavelengths," *J. Phys. Appl. Phys.*, vol. 42, no. 13, p. 133001, 2009.
[22] Y. Zhou, Q. Wen, Z. Wen, J. Huang, and F. Chang, "An electromagnetic scanning mirror integrated with blazed grating and angle sensor for a near infrared micro spectrometer," *J. Micromech. Microeng.*, vol. 27, no. 12, p. 125009, 2017.
[23] T. Pügner, J. Knobbe, and H. Grüger, "Near-infrared grating spectrometer for mobile phone applications," *Appl. Spectros.*, vol. 70, no. 5, pp. 734–745, 2016.
[24] A. Das, T. Swedish, A. Wahi, et al., "Mobile phone based mini-spectrometer for rapid screening of skin cancer," in *Next-Generation Spectroscopic Technologies, VIII*, Washington DC, International Society for Optics and Photonics, 2015, p. 94820M.
[25] L. Mertz, "Ultrasound? Fetal monitoring? Spectrometer? There's an app for that!: Biomedical smart phone apps are taking healthcare by storm," IEEE Pulse, vol. 3, no. 2, pp. 16–21, 2012.
[26] N.E. Samec, N.U. Robaina, A. Kaehler, et al., "Magic Leap," Augmented Reality Spectroscopy, Australia, AU2017331284A1, 2018.
[27] A. Burkart, S. Cogliati, A. Schickling, and U. Rascher, "A novel UAV-based ultra-light weight spectrometer for field spectroscopy," *IEEE Sensor. J.*, vol. 14, no. 1, pp. 62–67, 2013.
[28] S. K. von Bueren, A. Burkart, A. Hueni, U. Rascher, M. P. Tuohy, and I. Yule, "Deploying four optical UAV-based sensors over grassland: Challenges and limitations," *Biogeosciences*, vol. 12, no. 1, pp. 163–175, 2015.
[29] S. Natesan, C. Armenakis, G. Benari, and R. Lee, "Use of UAV-borne spectrometer for land cover classification," *Drones*, vol. 2, no. 2, p. 16, 2018.
[30] H. Saari, V. V. Aallos, A. Akujärvi, et al., "Novel miniaturized hyperspectral sensor for UAV and space applications," in *Sensors, Systems, and Next-Generation Satellites XIII*, Washington, International Society for Optics and Photonics, 2009, p. 74741M.
[31] E. Herrala and J. Okkonen, "Imaging spectrograph and camera solutions for industrial applications," in *Machine Vision for Advanced Production*, Singapore, World Scientific, 1996, pp. 43–54.
[32] E. Huang, Q. Ma, and Z. Liu, "Etalon array reconstructive spectrometry," *Sci. Rep.*, vol. 7, p. 40693, 2017.
[33] J. Correia, G. De Graaf, S. Kong, M. Bartek, and R. Wolffenbuttel, "Single-chip CMOS optical microspectrometer," *Sensor Actuator Phys.*, vol. 82, no. 1–3, pp. 191–197, 2000.
[34] A. Emadi, H. Wu, G. de Graaf, and R. Wolffenbuttel, "Design and implementation of a sub-nm resolution microspectrometer based on a Linear-Variable Optical Filter," *Optics Express*, vol. 20, no. 1, pp. 489–507, 2012.
[35] A. Emadi, H. Wu, G. de Graaf, P. Enoksson, J. H. Correia, and R. Wolffenbuttel, "Linear variable optical filter-based ultraviolet microspectrometer," *Appl. Optic.*, vol. 51, no. 19, pp. 4308–4315, 2012.
[36] A. Emadi, H. Wu, S. Grabarnik, et al., "Fabrication and characterization of IC-compatible linear variable optical filters with application in a micro-spectrometer," *Sensor Actuator Phys.*, vol. 162, no. 2, pp. 400–405, 2010.
[37] PYREOS, *Linear Arrays – Taking Lab Analysis Out into the Field*, Edinburgh, PYREOS, 2019. Available at: https://pyreos.com/linear-arrays.
[38] B. Craig, V. R. Shrestha, J. Meng, J. J. Cadusch, and K. B. Crozier, "Experimental demonstration of infrared spectral reconstruction using plasmonic metasurfaces," *Optic Lett.*, vol. 43, no. 18, pp. 4481–4484, 2018.
[39] U. Kurokawa, B. I. Choi, and C. C. Chang, "Filter-based miniature spectrometers: spectrum reconstruction using adaptive regularization," *IEEE Sensor. J.*, vol. 11, no. 7, pp. 1556–1563, 2011.
[40] B. J. Craig, J. Meng, V. R. Shrestha, J. J. Cadusch, and K. B. Crozier, "Mid-to long-wave infrared computational spectroscopy using a subwavelength coaxial aperture array," *Sci. Rep.*, vol. 9, no. 1, pp. 1–11, 2019.
[41] A. Wang and Y. Dan, "Mid-infrared plasmonic multispectral filters," *Sci. Rep.*, vol. 8, no. 1, p. 11257, 2018.
[42] Z. Wang, S. Yi, A. Chen, et al., "Single-shot on-chip spectral sensors based on photonic crystal slabs," *Nat. Commun.*, vol. 10, no. 1, pp. 1–6, 2019.
[43] W. Hartmann, P. Varytis, H. Gehring, et al., "Waveguide-integrated broadband spectrometer based on tailored disorder," *Adv. Optic. Mater.*, vol. 8, no. 6, p. 1901602, 2020.
[44] B. Redding, S. F. Liew, R. Sarma, and H. Cao, "Compact spectrometer based on a disordered photonic chip," *Nat. Photonics*, vol. 7 , no. 9, p. 746, 2013.
[45] J. Bao and M. G. Bawendi, "A colloidal quantum dot spectrometer," *Nature*, vol. 523, no. 7558, p. 67, 2015.
[46] Z. Yang, T. Albrow-Owen, and H. Cui, et al., "Single-nanowire spectrometers," *Science*, vol. 365, no. 6457, pp. 1017–1020, 2019.
[47] J. Meng, J. J. Cadusch, and K. B. Crozier, "Detector-only spectrometer based on structurally colored silicon nanowires and a reconstruction algorithm," *Nano Lett.*, vol. 20, no. 1, pp. 320–328, 2019.
[48] J. J. Cadusch, J. Meng, B. Craig, and K. B. Crozier, "Silicon microspectrometer chip based on nanostructured fishnet photodetectors with tailored responsivities and machine learning," *Optica*, vol. 6, no. 9, pp. 1171–1177, 2019.
[49] B. Redding, S.M. Popoff, and H. Cao, "All-fiber spectrometer based on speckle pattern reconstruction," *Optics Express*, vol. 21, no. 5, pp. 6584–6600, 2013.
[50] J.J. Cadusch, J. Meng, and K.B. Crozier, "Nanostructured fishnet silicon photodetector pixels as a fully-contained microspectrometer chip," in *CLEO: Science and Innovations*, Washington, Optical Society of America, 2018, p. SM2I.4.
[51] J. Oliver, W. Lee, S. Park, and H. N. Lee, "Improving resolution of miniature spectrometers by exploiting sparse nature of signals," *Optics Express*, vol. 20, no. 3, pp. 2613–2625, 2012.

[52] C. C. Chang and H. N. Lee, "On the estimation of target spectrum for filter-array based spectrometers," *Optics Express*, 16, no. 2, pp. 1056–1061, 2008.
[53] J. Oliver, W. B. Lee, and H. N. Lee, "Filters with random transmittance for improving resolution in filter-array-based spectrometers," *Optics Express*, 21, no. 4, pp. 3969–3989, 2013.
[54] Z. H. Zhou, Y. Jiang, Y. B. Yang, and S. F. Chen, "Lung cancer cell identification based on artificial neural network ensembles," *Artif. Intell. Med.*, 24, no. 1, pp. 25–36, 2002.
[55] A. Signoroni, M. Savardi, A. Baronio, and S. Benini, "Deep learning meets hyperspectral image analysis: a multidisciplinary review," *J. Imag.*, 5, no. 5, p. 52, 2019.